IBRACON Structures and Materials Journal
Revista IBRACON de Estruturas e Materiais
ISSN 1983-4195 ismj.org

ORIGINAL ARTICLE

Shear-torsion-bending interaction in RC beams according to NBR 6118/2014 and AASHTO LRFD 2014

Interação entre torção, flexão e cortante em vigas de concreto armado segundo NBR 6118/2014 e AASHTO LRFD 2014

Vinícius Belarmino Almeida[a]
Bernardo Horowitz[a]

[a]Universidade Federal de Pernambuco – UFPE, Centro de Tecnologia e Geociências, Programa de Pós-Graduação em Engenharia Civil, Recife, PE, Brasil

Received 4 October 2021
Accepted 7 March 2022

Abstract: Reinforced concrete beams are subjected to bending, torsion and shear simultaneously. The interaction of combined loading is complex and demands a unified model for analysis and design. Using the models from NBR 6118/2014 (variable angle truss model with parallel chords) and AASHTO LRFD Bridge Design Specifications 2014 (Modified Compression Field Theory), an algorithm was created, converting the resistance problem into a constrained optimization problem and generating an interaction surface that also displays the active constraints for each degree of interaction. Applying it to three beams previously tested, the experimental data was plotted against the surface obtained by the standards. The procedure and its optimization approach were efficient and effective in predicting the beams' resistance. Comparison between the interaction surfaces, empirical data and existing literature showed the procedure and the standards were consistent and its application simple and practical.

Keywords: reinforced concrete, bending, torsion, shear, interaction, optimization, NBR 6118, AASHTO LRFD.

Resumo: Vigas de concreto armado estão sujeitas a esforços de flexão, torção e cortante, muitas vezes simultaneamente. A interação entre esses é um fenômeno complexo, que exige um modelo unificado de análise e dimensionamento. Seguindo os modelos da NBR 6118/2014 (treliça generalizada de banzos paralelos) e AASHTO LRFD Bridge Design Specifications 2014 (Teoria do Campo de Compressão Modificada), implementou-se um algoritmo que transforma o problema de resistência em um problema de otimização com restrições, gerando uma superfície de interação com indicações das restrições ativas em cada grau de interação. Aplicando o procedimento para três vigas ensaiadas anteriormente, plotaram-se os resultados experimentais sobre a superfície obtida pelas normas. O procedimento e sua abordagem de otimização foram eficientes e eficazes em prever a resistência das vigas analisadas. A comparação das superfícies de interação com dados experimentais e resultados da literatura mostrou a consistência do procedimento e das normas, e sua aplicação se mostrou prática e simples.

Palavras-chave: concreto armado, flexão, torção, cortante, interação, otimização, NBR 6118, AASHTO LRFD.

How to cite: V. B. Almeida and B. Horowitz, "Shear-torsion-bending interaction in RC beams according to NBR 6118/2014 and AAASHTO LRFD 2014," *Rev. IBRACON Estrut. Mater.*, vol. 16, no. 1, e16102, 2023, https://doi.org/10.1590/S1983-41952023000100002

Corresponding author: Vinícius Belarmino Almeida. E-mail: vinicius.almeida@ufpe.br
Financial support: This study was financed in part by the Coordenação de Aperfeiçoamento de Pessoal de Nível Superior (CAPES) – Finance Code 001.
Conflict of interest: Nothing to declare.
Data Availability: The data that support the findings of this study are openly available in https://doi.org/10.48331/scielodata.ZGNEIO

1 INTRODUCTION

Reinforced concrete beams are subjected to bending, torsion and shear forces, with several mechanical and empirical models available for design and analysis considering each one of these separately. Most structural elements withstand a combined action, however. In order to analyze this interaction, many engineers resort to simplified procedures or completely ignore this phenomena, due to the complexity of standards procedures and the lack of unanimity around a straightforward mechanical and rational model [1].

While flexure theory has been around since the 17th century and is well established for reinforced concrete since the 1960s, the most popular model for shear and torsion (truss/strut-and-tie model) is relatively new, developed by Ritter and Morsch in the beginning of the 20th century. Even the most modern and complete models still carry some empiricism and needs some validation for some situations [2], [3]. Other than generalized truss models using equilibrium or compatibility, recent research has suggested different models such as trusses with crack friction, disturbed stress fields, finite element applications, simplified model for combined stress resultants and shear friction [4], [5].

The sheer number of variables involved in the shear problem make it very difficult for experiments to be interpreted. Also, shear and interaction tests are hard to perform in a practical and reliable manner. These factors combined hinder the proposal of a simple and complete method for analysis and design [6]. Compared to the flexure procedure, standards still use too many equations, suggest overconservative simplifications, or require the use of iterative methods for shear. The goal of this paper is to show an automatic method with an optimization approach that allows the use of the complete procedures proposed by two standards: NBR 6118/2014 and AASHTO LRFD 2014. The proposed algorithm generates full shear-torsion- bending interaction surfaces, allowing the verification of the standards consistency with experimental data from the literature.

2 PROPOSED METHOD

Given: T, M and V (torsion moment, bending moment and shear force) acting on a beam; r an action multiplier (a non-dimensional variable between 0 and 1 - the "magnitude" of forces); and F_{max} the maximum resistance of the force F acting alone; the geometric relationship shown in Figure 1 is obtained. α_r and β_r control the interaction between the actions, obtained by Equations 1, 2 e 3. To obtain the resistance of the section for an interaction degree (α_r and β_r), r must be maximized, increasing the actions until failure. This results in Problem 1 (Figure 2), where a constraint A (action) < R (resistance) represents a standard's verification.

$$M = M_{max} r sin\beta_r \tag{1}$$

$$T = T_{max} r cos\beta_r sin\alpha_r \tag{2}$$

$$V = V_{max} r cos\beta_r cos\alpha_r \tag{3}$$

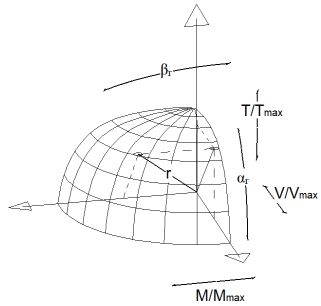

Figure 1: Relationship between torsion moment, bending moment and shear force.

Maximize	$\mathrm{r} = f(r, \alpha_r, \beta_r)$
$\mathrm{r} \in \mathbb{R} \mid \alpha_r, \beta_r \in [0, \frac{\pi}{2}]$	
Subject to:	$S(r, \alpha_r, \beta_r) \leq \mathrm{R}(r, \alpha_r, \beta_r)$

Figure 2: Subroutine for Problem 1.

This approach was taken from Obel [7], extended to 3D and solved using a SQP algorithm from commercial software MATLAB. The algorithms are available on SciELO Data [8].

3 STANDARDS' PROCEDURES

3.1 NBR 6118/2014

NBR 6118/2014 uses load and resistance factored design, with statistical coefficients for each limit state to consider variability, uncertainty, precision, simultaneity and importance of the phenomena analyzed. Thus, in the ultimate limit state, design must ensure the design action F_{Sd} is inferior to design resistance F_{Rd}. This section shows its prescriptions for shear, torsion, flexure and interaction in beams [9].

Shear

The standard allows two calculation models based on the generalized truss with parallel chords, considering concrete struts inclined at θ and transverse steel ties inclined at α with some concrete contribution in tension. Model II permits a variation of the inclination of the struts θ between 30º and 45º, while model I sets the angle of the diagonals at 45º, in a conservative simplification. Thus, this article will focus on the demonstration of Model II [9].

To check the **inclined concrete struts** between the diagonal cracks, vertical equilibrium is applied on the left section of Figure 3a and 3b, finding R_{cw}, the force on the struts as a function of the shear force V_{Sd} (Equation 4). The compression stress on the struts σ_{cw} is shown in Figure 3c and is given by Equation 5, using the beam width b_w and lever arm z.

$$R_{cw} = V_{Sd} / \, sin\theta \tag{4}$$

$$\sigma_{cw} = \frac{R_{cw}}{b_w \times z \times (cot\theta + cot\alpha) \times sin\theta} \tag{5}$$

Substituting Equation 4 in Equation 5, Equation 6 is obtained. At failure, the compression stress on the strut reaches concrete compression resistance, which is 70% of the usual maximum $0.85 f_{cd}$, due to the biaxial stress nature of the truss model. A reduction factor α_{v2} is considered, to adapt the cylinder test result that originates f_{cd} to the shape of the concrete struts (Equation 7). Assuming the lever arm z is 90% of the effective depth d, Equation 6 turns to Equation 8 (shear force. V_{Sd} reaches the strut shear resistance V_{Rd2}).

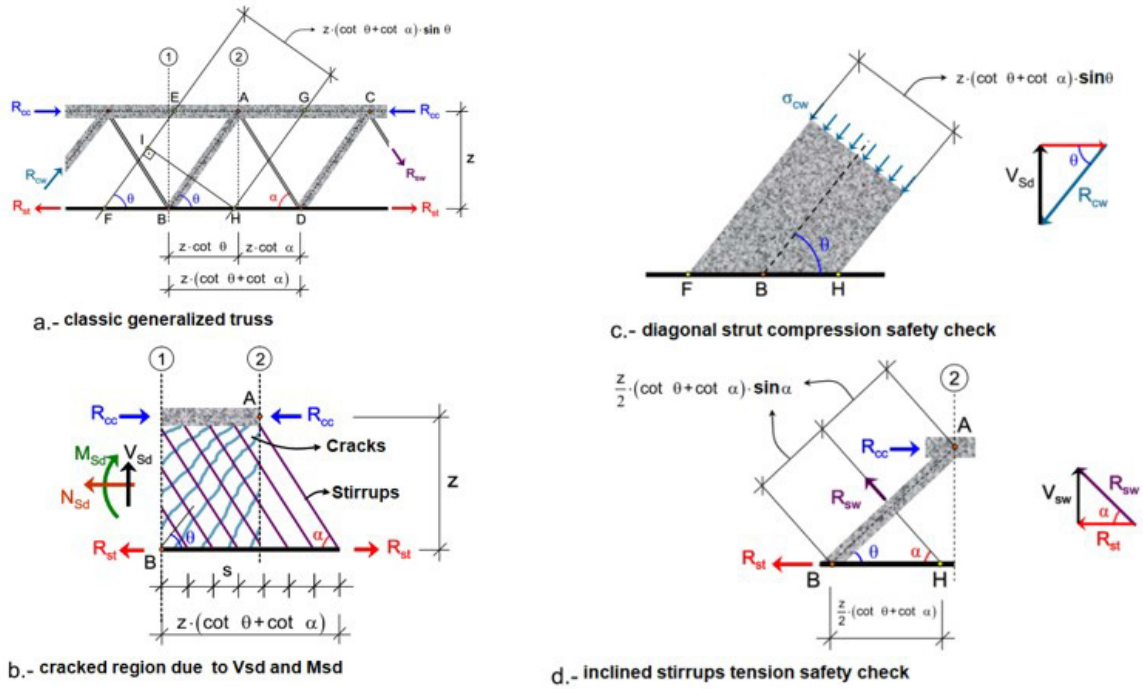

Figure 3: Generalized truss model with parallel chords [10].

$$\sigma_{cw} = \frac{V_{Sd}}{bw \times z \times (cot\theta + cot\alpha) \times sin^2\theta} \tag{6}$$

$$\alpha_{v2} = 1 - \frac{f_{ck}}{250} \tag{7}$$

$$V_{Sd} = V_{Rd2} = 0.54 \times \alpha_{v2} \times f_{cd} \times b_w \times d \times sin\,\theta^2 \times (cot\,\theta + cot\,\alpha) \tag{8}$$

The **ties** resist shear though a steel contribution V_{sw} and a concrete contribution V_{cw}. The force acting on the stirrups R_{swt} is obtained by vertical equilibrium on the right section of Figure 3b e 3d, resulting in Equation 9. Being the number of stirrups (spaced at s distance) crossing a diagonal crack n_{bars} given by Equation 10 and considering them to yield at f_{yd} stress, the maximum force developed by the vertical hoops is given by Equation 11. At failure, the force on the stirrups reaches the maximum possible force developed by the steel (Equation 12).

$$R_{swt} \times sin\alpha = V_{sw} \tag{9}$$

$$n_{bars} = \frac{z \times (cot\theta + cot\alpha)}{s} \tag{10}$$

$$R_{swt} = \frac{A_{sw} \times f_{yd} \times 0.9d \times (cot\theta + cot\alpha)}{s} \tag{11}$$

$$V_{sw} = \frac{A_{sw} \times f_{yd} \times 0.9d \times (cot\theta + cot\alpha) \times sin\alpha}{s} \quad (12)$$

Using a similar procedure on the sections from Figure 4, the concrete contribution V_{cw}, is given by Equation 13, as a function of the concrete tension design resistance f_{ctd}. This must be diminished, however, to account for the cracking of the section depending on the bending moment and relative shear force, according to Equations 14, 15 and 16. At failure, shear design force equals the shear resistance of the ties V_{Rd3} given by Equation 17, adding steel and concrete contribution.

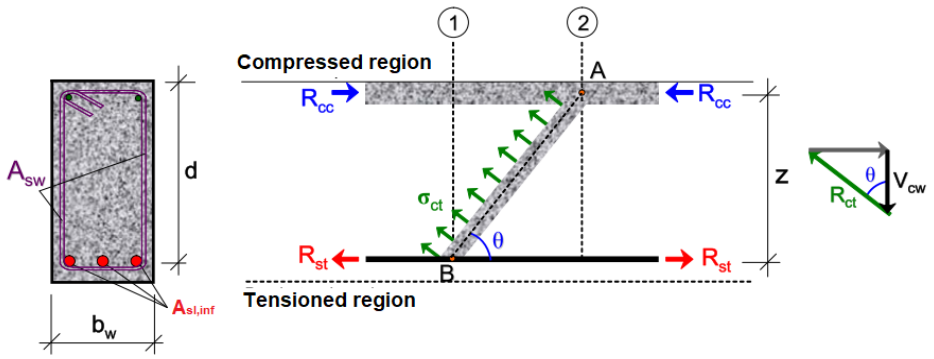

Figure 4: Concrete contribution to the ties [10].

$$V_{cw} = b_w \times 0.9d \times f_{ctd} \times \frac{cos\theta}{sin\theta} \quad (13)$$

$$V_{c0} = 0.6 \times f_{ctd} \times b_w \times d \quad (14)$$

$$V_{c1} = V_{c0} \times \frac{(V_{Sd} - V_{Rd2})}{(V_{c0} - V_{Rd2})} \quad (15)$$

$$V_c = \begin{cases} 0, for\ fully\ tensioned\ sections\ under\ flexure - tension \\ V_{c1}, for\ partially\ tensioned\ sections\ under\ flexure - tension \\ V_{c1} + \left(1 + \frac{M_0}{M_{Sd}}\right), for\ flexure - compression, being\ M_0\ the\ decompression\ bending \end{cases} \quad (16)$$

$$V_{Sd} = V_{Rd3} = V_{sw} + V_c \quad (17)$$

To verify the **parallel chords**, horizontal equilibrium is observed in Figure 3b, finding the force on the tensioned chord $R_{st,v}$ in Equation 18, which generates Equation 19 using previous equations. Also, the bending moment induces a tension force on the bottom chord, given by Equation 20. Thus, the bottom chord is tensioned by a force given by Equation 21. This force must be inferior to the yielding force of the bottom steel area $A_{sl,inf}$ (Equation 22).

$$2R_{st,v} = R_{cw} \times cos\theta - R_{sw} \times cos\alpha \tag{18}$$

$$R_{st,v} = V_{Sd}(cot\,\theta - cot\,\alpha)/2 \tag{19}$$

$$R_{st,m} = \frac{M_{Sd}}{z} \tag{20}$$

$$R_{st} = \frac{M_{Sd}}{z} + V_{Sd}(cot\,\theta - cot\,\alpha)/2 \tag{21}$$

$$\frac{M_{Sd}}{z} + 0.5V_{Sd}(cot\,\theta - cot\,\alpha) < f_{yd} \times A_{sl,inf} \tag{22}$$

Torsion

For torsion, NBR 6118/2014 considers a similar model: generalized space truss with parallel chords, considering inclined concrete struts and transverse steel ties without concrete contribution. The space truss geometry is obtained using the thin-walled tube analogy (Figure 5). The struts inclination must be compatible with the one assumed for shear, using either Model I or Model II, but the latter will be the focus of this article, for generalization [9].

The equivalent section is comprised of four perpendicular walls, comprised of connected plane trusses with diagonal struts, transverse steel ties and longitudinal steel parallel chords. Considering spalling of the section under torsion, the equivalent section is a function of the original dimensions, section perimeter u and the distance from the corner steel centroid to the lateral face (c_1). Its thickness h_e spans between values from Equation 23 and Equation 24. Its middle line perimeter u_e is given by Equation 25 and its enclosed area A_e is obtained from Equation 26.

$$h_{e,min} = \begin{cases} min\left(\frac{A_c}{u}, b_w - 2c_1\right), if\ \frac{A_c}{u} < 2c_1 \\ 2c_1, otherwise \end{cases} \tag{23}$$

$$h_{e,max} = \begin{cases} h_{e,min}, if\ \frac{A_c}{u} < 2c_1 \\ \frac{A_c}{u}, otherwise \end{cases} \tag{24}$$

$$u_e = \begin{cases} u - 8c_1, if\ \frac{A_c}{u} < 2c_1 \\ u - 4h_e, otherwise \end{cases} \tag{25}$$

$$A_e = \begin{cases} (b_w - 2c_1) \times (h - 2c_1), if\ \frac{A_c}{u} < 2c_1 \\ (b_w - h_e) \times (h - h_e), otherwise \end{cases} \tag{26}$$

Considering the shear flow on the wall q is the ratio of the shear stress over the wall thickness t and applying moment equilibrium, Equation 27 gives the relation between torsion and shear flow. The shear force is the product between the shear flow and its length, which leads to Equation 28 giving the shear force on the walls due to torsion.

Using a section of the vertical wall like Figure 6, and considering that the n_{bars} ties crossing a diagonal crack (Equation 29) yield at f_{ywd}, vertical equilibrium gives the maximum shear force resisted by each vertical wall (Equation 30). Applying Equation 28, the maximum torsion resisted by each leg A_t of the **stirrups** is given by Equation 31. The shear path enclosed area is taken as A_e. Concrete under tension doesn't contribute, due to cracking caused by torsion [11].

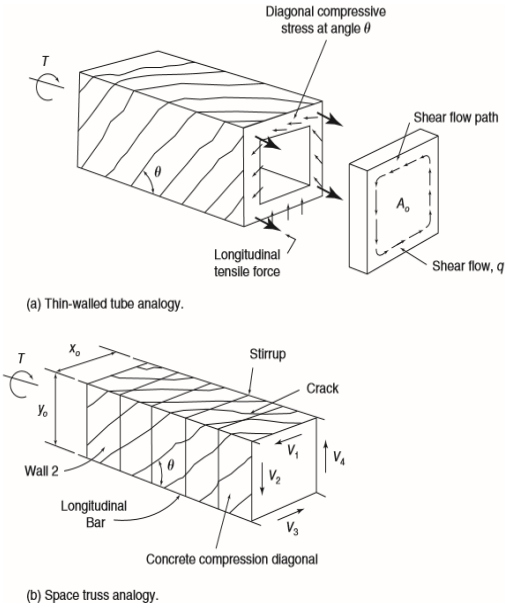

Figure 5: Thin-walled tube analogy and generalized space truss [12].

$$T = 2qA_0 \tag{27}$$

$$V1 = V3 = \frac{T}{2A_o} \times x_o \; e \; V2 = V4 = \frac{T}{2A_o} \times y_o \tag{28}$$

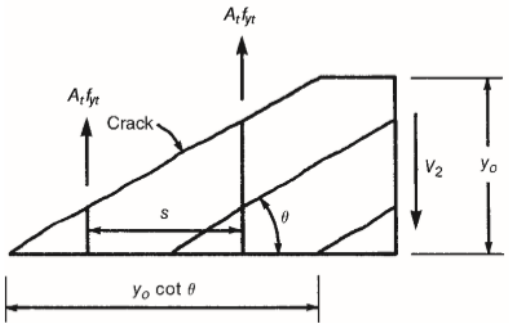

Figure 6: Section of the vertical wall detailing the stirrups force [12].

$$n_{bars} = \frac{y_o}{s} \times cot\theta \tag{29}$$

$$V_2 = \frac{A_t f_{ywd} y_o}{s} \times cot\theta \tag{30}$$

$$T_{Rd3} = \frac{2A_e A_t f_{ywd}}{s} \times cot\theta \tag{31}$$

Using a different section of the vertical walls (Figure 7), and using vertical and horizontal equilibrium, it is possible to obtain the compression force on struts D_2 (Equation 32) and the tension force on the chords N (Equation 33). Using Equation 28, these actions can be related to the torsion, resulting in (Equation 34) and (Equation 35). At failure, total steel area $A_{s,tot}$ of the **parallel chords** yield, giving the maximum torsion resisted by them T_{Rd4} (Equation 36). Assuming the same as for shear, at failure the **concrete struts** reach its strength, which gives its torsion resistance T_{Rd2} (Equation 37) [13].

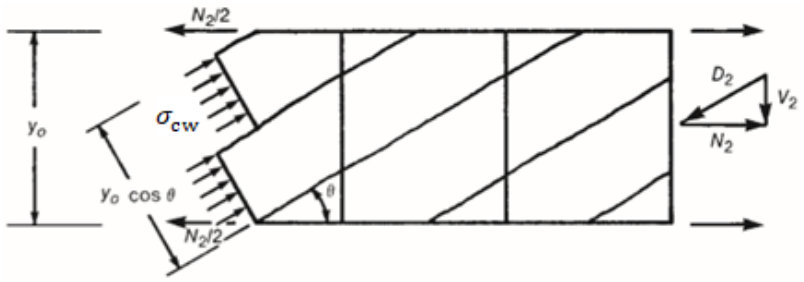

Figure 7: Section of a vertical wall of the truss detailing the chords and struts forces [12].

$$D_2 = \frac{V_2}{sin\theta} \tag{32}$$

$$N = 2(V_1\, cot\,\theta + V_2\, cot\,\theta) \tag{33}$$

$$N = \frac{T}{2A_0} 2(x_0 + y_0)\, cot\,\theta = \frac{T}{2A_0} p_o\, cot\,\theta \tag{34}$$

$$\sigma_{cw} = \frac{V_2}{t y_0\, cos\,\theta\, sin\,\theta} = \frac{\frac{T}{2A_0} \times y_o}{t y_0\, cos\,\theta\, sin\,\theta} = \frac{T}{2tA_0\, cos\,\theta\, sin\,\theta} \tag{35}$$

$$T_{Rd4} = \frac{2A_e A_{s,tot} f_{yd}\, tan\,\theta}{u_e} \tag{36}$$

$$T_{Rd2} = 0.5 \times \alpha_{v2} \times f_{cd} \times t \times A_e \times sin\,2\theta \quad (37)$$

In summary, torsion design according to NBR 6118/2014 aims to ensure that torsion design load T_{Sd} is inferior to the struts, ties and chords resistance T_{Rd2}, T_{Rd3} and T_{Rd4}.

Bending moment and interaction

The Brazilian standard uses flexure basic assumptions: plane sections remain plane, perfect steel-concrete bond and constitutive relationships for concrete and steel, neglecting the cracked concrete under tension. Failure is considered to happen under certain domains, where concrete maybe crushed, steel may yield or a combination of both (Figure 8) [9].

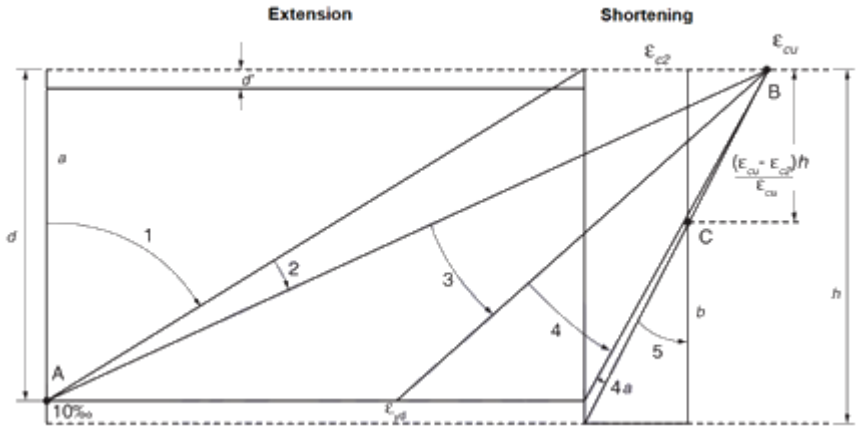

Figure 8: Failure domains for flexure [9].

In this article, domains 2 and 3 will be used to obtain bending resistance, where compressed concrete is crushed, and steel is beyond yielding strain. Maximum compression stress is approximated by a stress block and its height a is a fraction of the neutral line height c. The acting design bending moment M_{Sd} must be inferior to the bending developed by the compression-tension couple that act on the lever arm z. This may be considered 90% of the effective height d or a function of the stress block height, which gives the design bending resistance M_{Rd} (Equation 38). This process is illustrated by Figure 9 [14]

$$M_{Rd} = z \times f_{yd} A_{s,inf} = 0.9d \times f_{yd} A_{s,inf} \; or \; (d - \tfrac{a}{2}) \times f_{yd} A_{s,inf} \quad (38)$$

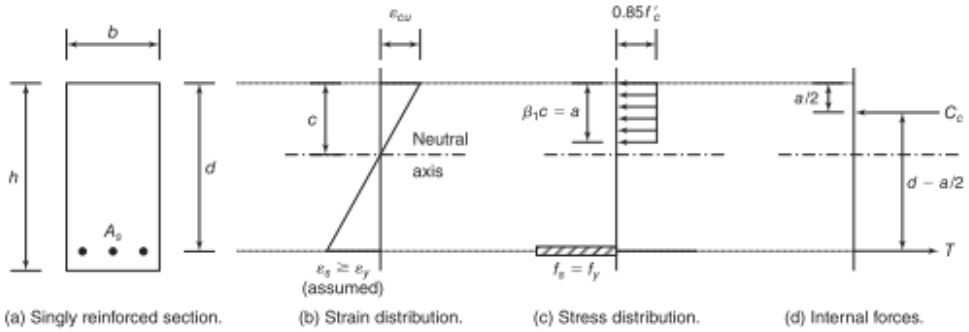

Figure 9: RC concrete cross section under flexure [12].

Due to the interaction of combined action, a triaxial stress state arises, with different levels of cracking, softening and strength for each region of the section, which would require a complex 3D model for an exact analysis. The model used by the Brazilian standard, however, is able to capture the phenomenon with a reasonable accuracy, combining the generalized space truss with parallel chords for shear and torsion with the flexure theory [13].

In the **diagonal concrete struts**, flexure influences only the inclination and the cracking level, reducing rigidity and strength. Torsion induces circulatory shear stress around the section, whereas shear force causes shear stress distributed on the web. In hollow sections, only the most critical wall is verified, where shear and torsion effects are added Figure 10a. In solid sections, this separation is impossible, and the real interaction is quite complex (Figure 10b). NBR 6118/2014 considers a linear interaction, as shown in Equation 39 [13].

Only shear and torsion induce stresses on the **ties**. These effects are added on one leg of the hoops and this linear superposition is accounted by Equation 40 simply adding the portion of the steel used by torsion (first term) and by shear (A_{sv}, where an relieve of the effect is considered in Equation 41, due to the concrete contribution to shear resistance) [7].

The **top chord** steel $A_{s,sup}$ is tensioned by shear and torsion and compressed by flexure (Equation 42), whereas the **bottom chord** steel $A_{s,inf}$ is tensioned by all actions (Equation 43) [12]. In highly compressed hollow sections, the principal stresses induced by the torsion shear stress and flexure compression becomes relevant and needs to be checked. Using Mohr's circle, the maximum principal stress σ_{cmax} is given by Equation 44, as a function of the average normal stress caused by bending σ_{cmed} (Equation 45) and shear stress due to torsion τ_t (Equation 46). The compression strength $\bar{f}_{cd12}$ can be taken as an average between strut-and-tie resistances f_{cd1} (only struts node) e f_{cd2} (strut and ties node), resulting in Equation 47. At failure, the principal stress must be smaller than the strength Equation 48.

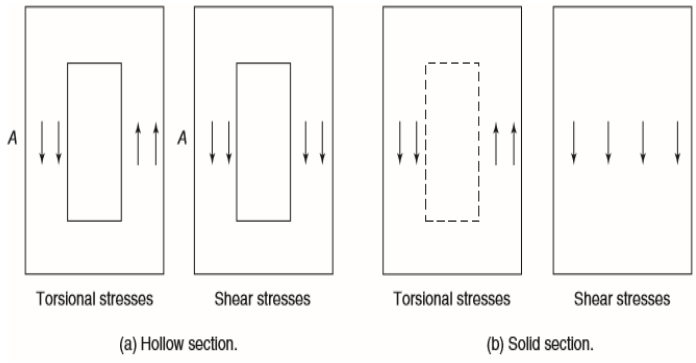

Figure 10: Shear and torsion stresses on a hollow and solid section [12].

$$\frac{T_{Sd}}{T_{Rd2}} + \frac{V_{Sd}}{V_{Rd2}} < 1 \tag{39}$$

$$\frac{T_{Sd}}{f_{ywd} \times A_e \times cot\,\theta} + A_{sv} < A_{sw}/s \tag{40}$$

$$A_{sv} = max(V_{Sd} - V_c, 0)/(f_{ywd} \times z \times cot\theta) \tag{41}$$

$$-\frac{M_{Sd}}{0.9d} + (0.5V_{Sd} + T_{Sd} \times u_e/4A_e)\,cot\,\theta < f_{yd} \times A_{s,sup} \tag{42}$$

$$\frac{M_{Sd}}{0.9d} + (0.5V_{Sd} + T_{Sd} \times u_e/4A_e)\, cot\, \theta < f_{yd} \times A_{s,inf} \tag{43}$$

$$\sigma_{cmax} = \frac{\sigma_{cmed}}{2} + \sqrt{\left(\frac{\sigma_{cmed}}{2}\right)^2 + \tau_t^2} \tag{44}$$

$$\sigma_{cmed} = \frac{M_{Sd}}{0.9d \times b_w \times 2(d - 0.9d)} \tag{45}$$

$$\tau_t = \frac{T_{Sd}}{2 \times t \times A_0} \tag{46}$$

$$\bar{f}_{cd12} = \lambda f_{cd1} + (1 - \lambda) f_{cd2}, where\ \lambda = cos\,\gamma\ \ and\ \gamma = arctan\left(\frac{{}^{T_{Sd}}/_{T_{max}}}{{}^{M_{Sd}}/_{M_{max}}}\right) \tag{47}$$

$$\sigma_{cmax} < \bar{f}_{cd12} \tag{48}$$

3.2 AASHTO LRFD Bridge Design Specifications 2014

The AASHTO LRFD 2014 standard uses a similar design approach to the Brazilian standard, with statistical coefficients that major loads and reduces resistance, aiming to ensure factored action F_u is inferior to the nominal resistance F_n. This section shows its prescriptions for shear, torsion, flexure and interaction, taken from the standard's chapters 5.7 e 5.8 [15].

Shear

The standard's model for shear is based on the Modified Compression Field Theory (MCFT), which is a set of equilibrium, compatibility and constitutive relations created to give the complete response of cracked concrete under shear in the generalized truss. It considers parallel chords, tensioned ties and a continuous field of diagonal compression. Assuming the direction of principal stresses is the same of the strains and using both average and local stresses and strain, it achieves the set of equations in Figure 11. AASHTO uses a simplified version of MCFT, assuming the stresses in the cracked region are critical to failure and steel must yield to ensure ductility at failure. Shear resistance is then given by Equation 49, which accounts for a **stirrup's contribution** and a **concrete contribution** (using the β parameter for "aggregate interlock" and compression field inclination θ). Due to the nature of the "aggregate interlock" mechanism, this equation is restricted to f'_c< 64 MPa and a lightweight-aggregate reduction factor λ is considered. The lever arm may be taken as the maximum between 0.9d e 0.72h. To ensure stirrups yield before **crushing of struts**, an upper bound of 25% of the concrete compression resistance f'_c is set for shear stress [16]. These simplifications allow the equation to emulate the empirical "concrete and steel" contribution formula ($V_c + V_s$), traditional in the American standards and practice [1].

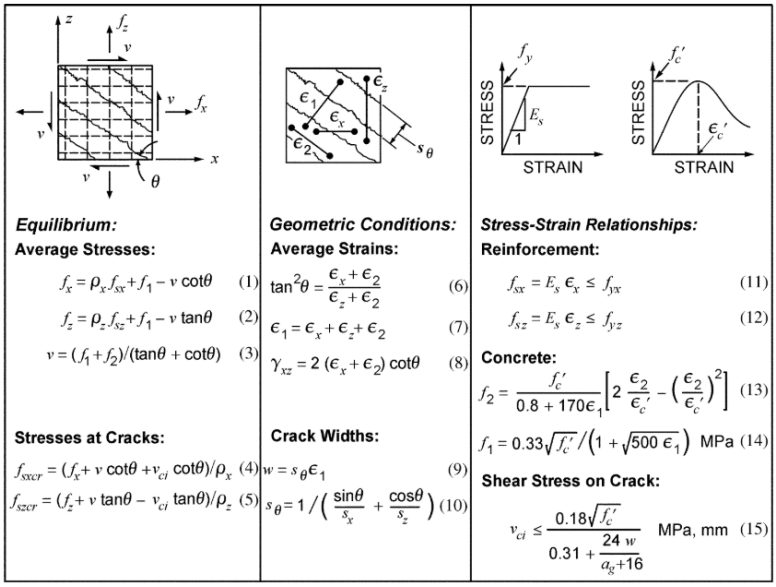

Figure 11: MCFT equilibrium, compatibility and constitutive relationships [16].

$$\frac{V_u}{b_w z} < \frac{V_n}{b_w z} = \frac{V_c + V_s}{b_w z} = \lambda\beta\sqrt{f'_c} + \frac{A_{sw} f_{ywd} cot\theta}{b_w s} < 0.25 f'_c \tag{49}$$

The β parameter accounts for several effects. Steel longitudinal strain ε_s accounts for the "strain effect", section's reinforcement ratio, level of shear, compression and bending action and rigidity E_s. It is obtained by Equation 50 using horizontal equilibrium (Figure 12), considering the compressed concrete to be uncracked and taking, conservatively, $0.5cot\theta$ as 1. Spacing between diagonal cracks s_x increases the crack width w and reduces the "aggregate interlock". This is called "size effect" and is given by Equation 51. Considering an aggregate size correction factor, s_{xe} is obtained, as shown in Equation 52. For high strength concrete, another correction is necessary, as the cracks tend to form through the aggregate. Based on empirical evidence for a diagonally cracked standard beam, the crack width is given as a function of longitudinal strain in Equation 53. To avoid negative values in this equation, a lower bound is set to Equation 50. Correcting Equation 53 to consider "size effect" and using it into the shear stress on crack considered my MCFT, Equation 54 is obtained [17].

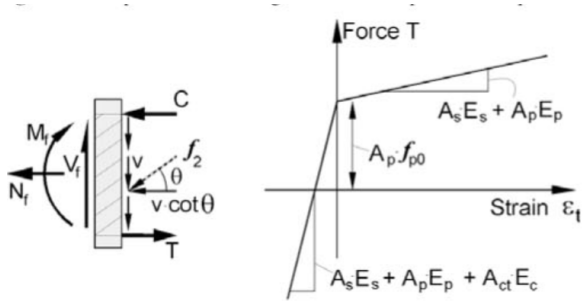

Figure 12: Acting and resisting forces and strains on a section [16].

$$-4 \times 10^{-4} < \varepsilon_s = \frac{\frac{M_u}{z} + 0.5V_u cot\theta + 0.5N_u}{A_{s,inf} \times E_s} = \frac{\frac{M_u}{z} + V_u + 0.5N_u}{A_{s,inf} \times E_s} < 6 \times 10^{-3} \tag{50}$$

$$s_x = \begin{cases} z, without\ stirrups \\ 0.3m, with\ stirrups \end{cases} \quad (51)$$

$$s_{xe} = s_x \times \frac{0.035}{0.016 + a_g} > 0.85 s_x \quad (52)$$

$$w = 0.2 + 2000\varepsilon_s \quad (53)$$

$$\beta = \frac{4.8}{(1+750\varepsilon_s)} \times \frac{1.3}{1+s_{xe}} \quad (54)$$

The compression field inclination θ defines the truss' capacity to redistribute forces to the ties and chords. For the steel to yield before the concrete crushes at failure, this angle must be within the limits shown in Figure 13. The inclination is assumed a linear function of the longitudinal strain, as in Equation 55. To control this redistribution in the truss, an upper bound is set to the angle, though the maximum limit on Equation 50.

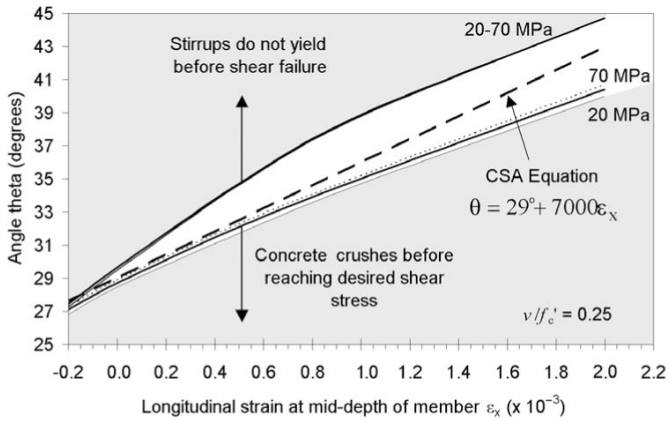

Figure 13: Inclination of the compression field as a function of longitudinal deformation [17].

$$\theta = 29° + 3500\varepsilon_s \quad (55)$$

The **bottom chord** of the truss must also be checked, ensuring tension due to shear and flexure aren't higher than the reinforcement's yield, which leads to Equation 56 [16].

$$f_{yd} \times A_{s,inf} > \frac{M_u}{z} + (V_u - 0.5V_s)cot\theta + 0.5N_u \quad (56)$$

Torsion

Simplified MCFT also accounts for torsion, aided by the thin-walled tube analogy. Its geometry considers spalling of the concrete cover and is a function of the original dimensions and the distance from the stirrups to the lateral face

of the section (c_2). Based on that, the enclosed area A_0 and perimeter p_0 of the shear flow middle line are taken respectively as 85% and 90% of the enclosed area A_{oh} and perimeter p_{h} of the hoops. AASHTO [15] uses the equilibrium of the generalized space truss to check for tension on the **ties** and **chords** (Equations 57 and 58). Crushing of the concrete **struts** is verified using a factored equivalent shear $V_{u,eq}$, considering a quadratic interaction between torsion and shear, that must be lower than $0.25f'_c b_w z$ (Equation 59). Since MCFT doesn't consider a concrete contribution to torsion resistance, only the parameters ε_s e θ are needed, calculated as previously shown for shear [18].

$$T_n = \frac{2A_o A_t f_{yt}}{s} \times cot\theta \tag{57}$$

$$\frac{M_u}{z} + \frac{0.45T_u p_h}{2A_o} \times cot\theta < f_{yd} \times A_{s,inf} \tag{58}$$

$$V_{u,eq} = \sqrt{{V_u}^2 + \left(\frac{0.9T_u p_h}{2A_o}\right)^2} < 0.25 \times f'_c \times b_w \times z \tag{59}$$

Flexure and interaction

Flexure is checked similarly to the Brazilian standard, resulting in Equation 60 [15].

$$M_n = z \times f_{yd} A_{s,inf} = 0.9d \times f_{yd} A_{s,inf} \; or \; 0.72h \times f_{yd} A_{s,inf} \tag{60}$$

Interaction on AASHTO affects the equilibrium verifications and β and θ, through the longitudinal strain. However, it uses a simplified version of MCFT. Spalling is rarely observed in sections with smaller cover, which leads to overestimated torsional stresses. The shear stress limit on the struts is also overconservative for beams with lower longitudinal strains [19].

Crushing of the **struts** in interaction is already verified in Equation 59. Tension on the **ties** is checked by superposition of shear and torsion in Equations 61 e 62. On the **chords**, a quadratic interaction is considered between shear and torsion, added to the compression or the tension caused by bending, as in Equations 63 e 64 [18]. Principal stresses are not checked on the top chord for solid sections, leaving such verification for a specific hollow section topic.

$$\frac{T_u}{f_{ywd} \times A_o \times cot\,\theta} + A_{sv} < A_{sw}/s \tag{61}$$

$$A_{sv} = max(V_u - V_c, 0)/(f_{ywd} \times z \times cot\theta) \tag{62}$$

$$\frac{M_u}{z} + \left(\sqrt{\left(\frac{0.45T_u p_h}{2A_o}\right)^2 + (V_u - 0.5 \times V_s)^2}\right) \times cot\theta < f_{yd} \times A_{s,inf} \tag{63}$$

$$-\frac{M_u}{z} + \left(\sqrt{\left(\frac{0.45T_u p_h}{2A_o}\right)^2 + (V_u - 0.5 \times V_s)^2}\right) \times cot\theta < f_{yd} \times A_{s,sup} \tag{64}$$

3.3 Optimization problem for each standard

NBR 6118/2014

For an interaction degree α_r and β_r, with unity values for resistance and load factors:

1) Given a RC beam with the following parameters:
   a. Longitudinal and transverse reinforcement yield stresses: f_{yd}, f_{ywd}
   b. Concrete compressive strength: $f_{cd} = f_{ck}$
   c. Cross section dimensions: b_w, h, d, c_1
   d. Longitudinal and transverse reinforcement detailing $A_{s,inf}, A_{s,sup}, A_{sw}, s$
2) Auxiliary parameters are calculated:
   a. Concrete average tensile strength (Equation 65):

$$f_{ct,m} = \begin{cases} 0.3 \times {f_{ck}}^{2/3}, if\ f_{ck} \leq 50MPa \\ 2.12 \times ln(1 + 0.11 f_{ck}), otherwise \end{cases} \quad (65)$$

   b. Concrete minimum tensile strength (Equation 66):

$$f_{ctk,inf} = 0.7 f_{ct,m} \quad (66)$$

   c. Concrete struts strength reduction factor α_{v2} - Equation 7
   d. Cross section's area A_c, moment of inertia I_c and perimeter u
   e. Thin-walled tube thicknesses ($h_{e,min}$) and ($h_{e,max}$) - Equations 23 and 24
3) Max resistance V_{max}, T_{max} e M_{max} are calculated as V_{Rd2} (Equation 8), T_{Rd2} (Equation 37) and M_{Rd} (Equation 38)
4) Objective function is defined as the action multiplier *r* (Equation 67):

$$f(r, \alpha_r, \beta_r, h_e, \theta) = r \quad (67)$$

5) The following variables are defined:
   a. Actions M_{Sd}, T_{Sd} *e* V_{Sd} according to Equations 1, 2 and 3
   b. Average strut-and-tie compressive resistance $\bar{f}_{cd12}$ as in Equation 47
   c. Thin-walled tube's middle line perimeter (u_e) and enclosed area (A_e) according to Equations 25 and 26
6) Constraints on the optimization variables are defined (Equations 68 and 69):

$$30° \leq \theta \leq 45° \quad (68)$$

$$h_{e,min} \leq h_e \leq h_{e,max} \quad (69)$$

7) Resistance constraints are defined:
   a. $T_{Sd} < T_{Rd2}, T_{Rd3}, T_{Rd4}$ according to Equation 31, Equation 35 and Equation 37
   b. $V_{Sd} < V_{Rd2}, V_{Rd3}$ according to Equation 8 and Equation 17
   c. Flexure and interaction check on the chords according to Equation 42 and Equation 43
   d. Verification of struts and ties according to Equation 39 and Equation 40
   e. Principal compressive stress check (Equation 48)
8) The objective function is maximized subject to constraints, using actions normalized by the maximum resistance. This procedure is shown on Problem 2 (Figure 14) and its MATLAB algorithm is available on SciELO Data RIEM repository as *Otim_R_NBR* [8].

Given: $f_{yd}, f_{ywd}, f_{cd}, b_w, \mathrm{h}, c_1, A_{s,inf}, A_{s,sup}, A_{sw}, s$

Considering:

$$V_{Rd2} = 0.54 \times \alpha_{v2} \times f_{cd} \times b_w \times d \times \sin\theta^2 \times (\cot\theta + \cot\alpha)$$

$$V_{Rd3} = V_{sw} + V_c = \frac{A_v f_{yt} 0.9d}{s} \times cot\theta + 0.6 \times f_{ct} \times b_w \times d$$

$$h_{e,min} = \begin{cases} \min\left(\frac{A_c}{u}, b_w - 2c_1\right), if\ \frac{A_c}{u} < 2c_1 \\ 2c_1,\ otherwise \end{cases}$$

$$h_{e,max} = \begin{cases} h_{e,min}, if\ \frac{A_c}{u} < 2c_1 \\ \frac{A_c}{u},\ otherwise \end{cases}$$

$$T_{Rd2} = 0.5 \times \alpha_{v2} \times f_{cd} \times A_e \times h_e \times \sin 2\theta$$

$$T_{Rd3} = A_{sw} \times f_{ywd} \times A_e \times \cot\theta / s$$

$$T_{Rd4} = 4 \times A_s \times f_{yd} \times A_e \times \frac{\tan\theta}{u_e}$$

$$\sigma_{cmax} = \frac{\sigma_{cmed}}{2} + \sqrt{\left(\frac{\sigma_{cmed}}{2}\right)^2 + \tau_t^2}$$

$$\bar{f}_{cd12} = \lambda f_{cd1} + (1-\lambda) f_{cd2}, where\ \lambda = cos\,\gamma\ and\ \gamma = arctg\left(\frac{T_{Sd}/T_{max}}{M_{Sd}/M_{max}}\right)$$

$$A_{sv} = \max(V_{Sd} - V_c, 0)/(f_{ywd} \times z \times cot\theta)$$

Maximize

$$f(\mathrm{r}, \alpha_r, \beta_r, h_e, \theta) = \mathrm{r}$$

$\mathrm{r}, h_e, \theta \in \mathbb{R}$
$\alpha_r, \beta_r \in [0, \pi/2]$

$$M_{Sd} = M_{max}\, r sin\beta_r; T_{Sd} = T_{max}\, r cos\beta_r sin\alpha_r; V_{Sd} = V_{max}\, r cos\beta_r cos\alpha_r$$

Subject to:

$$30° \le \theta \le 45°$$

$$h_{e,min} \le h_e \le h_{e,max}$$

$$T_{Sd} < T_{Rd2}, T_{Rd3}, T_{Rd4}$$

$$V_{Sd} < V_{Rd2}, V_{Rd3}$$

$$-M_{Sd}/0.9d + (0.5V_{Sd} + T_{Sd} \times u_e/4A_e)\cot\theta < f_{yd} \times A_{s,\,superior}$$

$$M_{Sd}/0.9d + (0.5V_{Sd} + T_{Sd} \times u_e/4A_e)\cot\theta < f_{yd} \times A_{s\,inferior}$$

$$\frac{T_{Sd}}{T_{Rd2}} + \frac{V_{Sd}}{V_{Rd2}} < 1$$

$$\sigma_{cmax} < f_{cd1-2}$$

$$\frac{T_{Sd}}{f_{ywd} \times A_e \times \cot\theta} + A_{sv} < A_{sw}/s$$

Figure 14: Subroutine for Problem 2.

AASHTO LRFD BRIDGE DESIGN SPECIFICATIONS 2014

For an interaction degree α_r and β_r, with unity values for resistance and load factors:

1) Given a RC beam with the following parameters:
   a. Longitudinal and transverse reinforcement yield stresses and Young's Modulus: $f_y, f_{yw}, E_s (\cong 210GPa)$
   b. Concrete compressive strength: f'_c
   c. Cross section dimensions: b_w, h, d, c_2
   d. Longitudinal and transverse reinforcement detailing $A_{s,inf}, A_{s,sup}, A_{sw}, s$
   e. Max aggregate size a_g (linearly reduced if $60\mathrm{MPa} < f'_c < 70\mathrm{MPa}$)
2) Auxiliar parameters are calculated:
   a. Stirrup's enclosed area A_{oh} and perimeter p_h
   b. Thin-walled tube's middle line enclosed area A_o and perimeter p_o taken respectively as 85% of A_{oh} and 90% of p_h
   c. Lever arm z taken as max between 90% of d and 72% of h
   d. Effective diagonal cracks spacing s_{xe} according to Equation 52

3) Max resistance V_{max}, T_{max} e M_{max} are taken as the upper bound of (Equation 49) for shear and torsion and maximum of (Equation 38) for the bending moment
4) Objective function is defined as the action multiplier *r* (Equation 70):

$$f(r, \alpha_r, \beta_r) = r \tag{70}$$

5) The following variables are defined:
   a. Factored actions M_u, T_u *e* V_u according to Equations 1, 2 and 3
   b. Factored equivalent shear force $V_{u,eq}$ according to Equation 59
   c. Longitudinal reinforcement strain ε_s (Equation 50), struts inclination θ (Equation 55) and "aggregate interlock" parameter β (Equation 54)
6) Resistance constraints are defined:
   a. Flexure and interaction check on the chords according to Equation 63 and Equation 64
   b. Shear, torsion and interaction verifications on the ties and the struts according to Equations 59 and 61
7) The objective function is maximized subject to constraints, using actions normalized by the maximum resistance. This procedure is shown on Problem 3 (Figure 15) and its implementation on MATLAB is available on the SciELO Data RIEM repository as *Otim_R_AASHTO* [8].

Given: $f_{yd}, f_{ywd}, f_{cd}, b_w, h, c_2, A_{s,inf}, A_{s,sup}, A_{sw}, s, a_g$

Considering:

$$A_o = 0.85 A_{oh} \text{ and } p_o = 0.9 p_h$$

$$A_{sv,min} = 0.083 \times \sqrt{f'_c} \times b_w \times s / f_{ywd}$$

$$s_x = \begin{cases} z, \text{ if } A_{sw} \geq A_{sv,min} \\ 0.3m, \text{if } A_{sw} < A_{sv,min} \end{cases}$$

$$s_{xe} = s_x \times \frac{0.035}{0.016 + a_g} > 0.85 s_x$$

$$V_{u,eq} = \sqrt{{V_u}^2 + \left(\frac{0.9 T_u p_h}{2A_o}\right)^2}$$

$$-4 \times 10^{-4} \leq \varepsilon_s = \frac{\frac{M_u}{z} + V_{u,eq}}{A_{s,inf} \times E_s} \leq 6 \times 10^{-3}$$

$$\beta = \frac{4.8}{(1 + 750\varepsilon_s)} \times \frac{1.3}{1 + s_{xe}}$$

$$\theta = 29° + 3500\varepsilon_s$$

$$V_c = 0.083 \times \beta \times \sqrt{f'_c} \times b_w \times z | V_s = \frac{A_{sw} f_{ywd} \cot\theta}{b_w s}$$

$$A_{sv} = \max(V_u - V_c, 0) / (f_{ywd} \times z \times \cot\theta)$$

Maximize $f(r, \alpha_r, \beta_r) = r$

$r \in \mathbb{R} \mid \alpha_r, \beta_r \in [0, \pi/2]$ $\quad M_u = M_{max} r \sin\beta_r ; T_u = T_{max} r \cos\beta_r \sin\alpha_r ; V_u = V_{max} r \cos\beta_r \cos\alpha_r$

Subject to:

$$\frac{T_u}{A_o f_{ywd} \cot\theta} + A_{sv} < \frac{A_v}{s}$$

$$V_{u,eq} < 0.25 \times f'_c \times b_w \times z$$

$$\frac{M_u}{z} + \left(\sqrt{\left(\frac{0.45 T_u p_h}{2A_o}\right)^2 + (V_u - 0.5 \times V_s)^2}\right) \times \cot\theta < f_{yd} \times A_{s,inf}$$

$$-\frac{M_u}{z} + \left(\sqrt{\left(\frac{0.45 T_u p_h}{2A_o}\right)^2 + (V_u - 0.5 \times V_s)^2}\right) \times \cot\theta < f_{yd} \times A_{s,sup}$$

Figure 15: Subroutine for Problem 3.

3.4 Post-processing

Based on the optimization's solution point and previous equations, the trio of resistance values for each interaction degree α_r and β_r is obtained. These values are then divided by the maximum resistance found for each kind. For each beam, several α_r and β_r are evaluated, ranging from 0º to 90º in 6º steps, obtaining enough points to plot a smooth interaction surface using interpolation. For comparison, experimental data points from the analyzed tests are plotted along with hidden lines starting from the origin. These were normalized using the maximum predicted resistance based on the tested beam's parameters, which may differ from nominal values. The scaling values were obtained by the programs *MVTmax_NBR* e *MVTmax_AASHTO*, available in [8]. Also, the algorithm calculates the value of the constraints at the solution, indicating the active one on the plot using a color code.

This post-processing procedure was also implemented in MATLAB and is available on the author's SciELO Data RIEM repository as *Pos_OtimR_NBR_AASHTO* [8].

4 COMPARISON WITH EXPERIMENTS

4.1 Analyzed tests

The first analyzed experiment was done by Badawy et al. [20], in which seven straight beams (S1 to S7) were tested under combined action until failure, as shown in Figure 16. The test region of the beams had the cross section shown in Figure 17. Other parameters are summarized on Table 1 and test results are shown in Table 2.

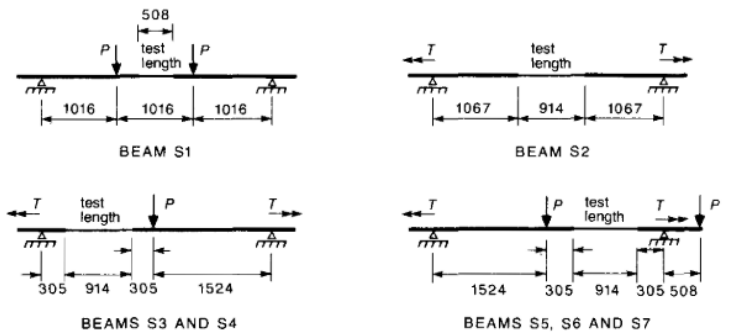

Figure 16: Test setup for combined action on beams S1 to S7 (dimensions in mm) [20].

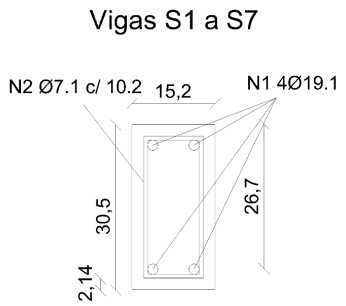

Figure 17: S1 to S7 beams cross section (dimensions in cm and bars diameter in mm).

The second analyzed experiment was done by McMullen and Warwaruk [21], in which 34 beams were tested under combined action until failure, comprising 7 groups with different reinforcement. Groups 5, 6 and 7, hereby called M5, M6 and M7 were the only tested under torsion, shear and bending. They were setup as shown in Figure 18 and had cross sections like those of Figure 19. As top and bottom reinforcement had different steel grades, the top reinforcement area will be multiplied by $\frac{f_{y,sup}}{f_{y,inf}}$ and bottom reinforcement strength will be used. Other parameters are summarized on Table 1 and test results are shown in Table 2.

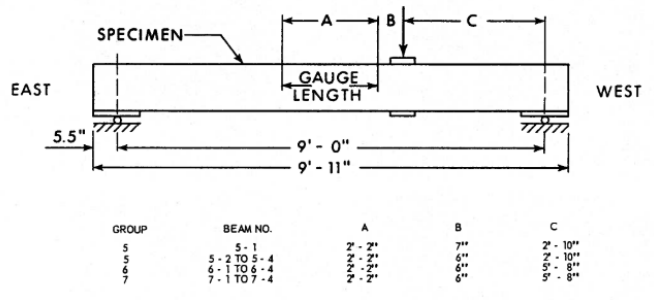

Figure 18: Test setup for combined action on beams M5 a M7 [21].

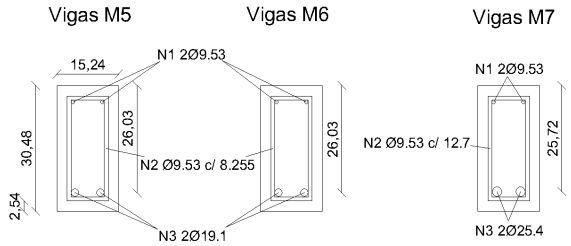

Figure 19: M5 to M7 beams cross section (dimensions in cm and bars diameter in mm).

Table 1: Other beams' parameters [20], [21]. *Areas multiplied by $\frac{fydsup}{fydinf}$

Beams	S1 a S7	M5	M6	M7
$f_{yd,inf}$ (MPa)	475	323.4	323.4	302.0
$f_{yd,sup}$ (MPa)	475	365.4	365.4	365.4
f_{ywd} (MPa)	300.3	370.25	370.25	370.25
f_{cd} (MPa)	30	34.47	34.47	34.47
b_w (cm)	15.2	15.24	15.24	15.24
h (cm)	30.5	30.48	30.48	30.48
d (cm)	26.7	26.03	26.03	25.72
c_1 (mm)	38	44.75	44.75	47.63
c_2 (mm)	24.95	30.16	30.16	30.16
$A_{s,inf}$ (cm2)	5.73	5.73	5.73	10.13
$A_{s,sup}$ (cm2)	5.73	1.61*	1.61*	1.73*
A_{sw} (cm2)	0.79	1.43	1.43	1.43
s (cm)	10.2	8.255	8.255	12.7
A_g (mm)	19	19	19	19

Table 2: Test results [20], [21].

Beams	M_{exp} (kN · m)	T_{exp} (kN · m)	V_{exp} (kN)	$b_{w,exp}$ (cm)	h_{exp} (cm)	f_{ccexp} (MPa)
S1	76.82	0.00	0.00	15.2	30.5	30
S2	0.00	13.56	0.00	15.2	30.5	30
S3	18.81	12.42	23.13	15.2	30.5	30
S4	51.51	10.73	50.71	15.2	30.5	30
S5	0.00	0.00	151.20	15.2	30.5	30
S6	0.00	8.93	93.41	15.2	30.5	30
S7	0.00	11.65	48.93	15.2	30.5	30
M5-1	7.34	14.46	3.38	15.88	30.81	39.37
M5-2	16.16	15.93	8.41	16.21	30.81	43.92
M5-3	31.41	14.69	17.21	15.24	30.81	41.78
M5-4	43.95	11.19	24.51	15.88	30.81	39.99
M6-1	7.34	14.57	8.05	15.88	30.81	40.40
M6-2	16.83	16.38	18.99	15.09	30.81	40.89
M6-3	29.83	14.91	34.12	15.88	30.81	39.30
M6-4	48.24	12.09	55.38	16.21	30.81	39.44
M7-1	6.33	12.65	6.94	15.09	30.81	41.92
M7-2	12.99	12.99	14.77	15.88	30.81	35.92
M7-3	31.07	14.91	36.07	16.21	30.81	39.30
M7-4	57.06	14.12	66.59	15.09	30.81	36.82

4.2 Results and discussion

S1 to S7 beams

Running the optimization and post-processing algorithms for the beams from Badawy et al. [20], the interaction surfaces were obtained for both standards (Figure 20). These were compared with the AASHTO interaction diagram for the same beams taken from Rahal [19] for validity, shown in Figure 21. The shape and magnitude of the surface is similar, although the drawing projection and the scaling factors were different from the ones used in this article. Due to some inconsistencies between Rahal's interaction surface and Badawy's experimental results, results S5, S6 and S7 were omitted from Rahal's interaction surface when used for validation.

Most of the surface is limited by yielding of ties, with an almost "conical" interaction (circular shear-torsion interaction, with decreasing radius following bending increase). Only with high flexure levels, chord resistance is critical. On AASHTO surface, the active constraint is yielding on the bottom chord. On the NBR diagram, the principal compressive stress check on the top chord was critical. This "extra" constraint prescribed by NBR 6118 chops the tip of the interaction surface when compared to the AASHTO's surface.

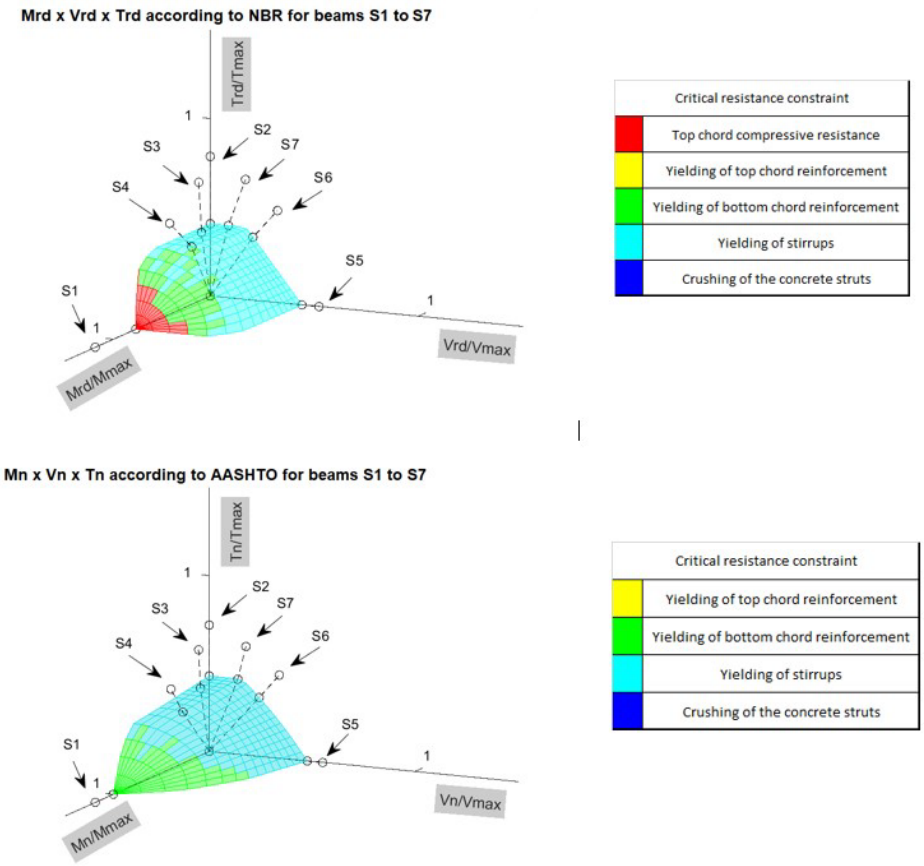

Figure 20: Interaction surface according to NBR and AASHTO for beams S1-S7.

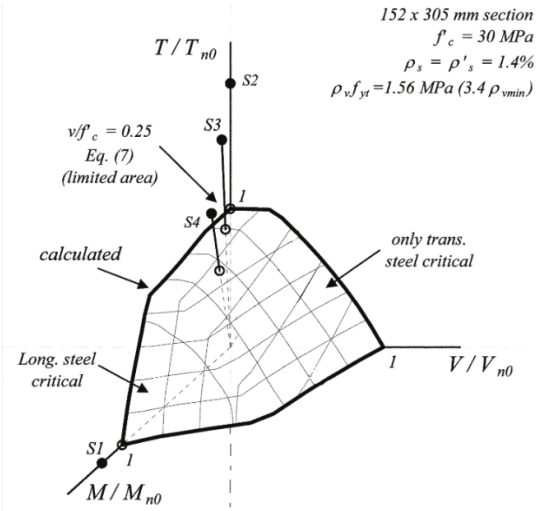

Figure 21: Adapted from Rahal's AASHTO surface for beams S1-S4 [19].M5 to M7 beams.

Running the optimization and post-processing algorithms for the beams from McMullen and Warwaruk [21], the interaction surfaces were obtained for both standards (Figure 22 for groups M5 and M6 and Figure 23 for group M7). On these beams, it

was observed a region on the surface (for low levels of flexure) which was limited by the yielding of the top chord, due to a weak top reinforcement. At this area, small increments on the bending moment led to an increase in torsion resistance, as the flexure compression alleviates the tension on the chord. This had been observed in similar situations by Onsongo [22].

For medium levels of flexure, resistance is limited by yielding of ties according to both standards. Beams M5 and M6, with weaker longitudinal reinforcement, show yielding of the bottom chord as critical even on this region, whereas beams M7 have this constraint as critical only in high levels of flexure. On either case, this interaction rapidly escalates for higher bending moments, causing a drastic reduction in shear and torsion resistance. For beams M7, the verification of compressive principal stresses on the top chord is once again critical according to NBR, predicting lower flexure resistance than AASHTO.

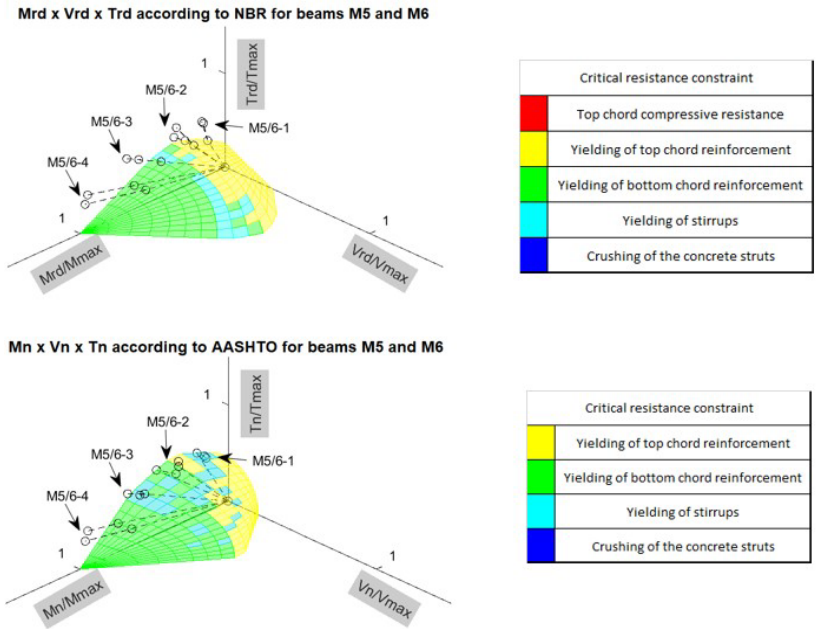

Figure 22: Interaction surface according to NBR and AASHTO for beams M5 e M6.

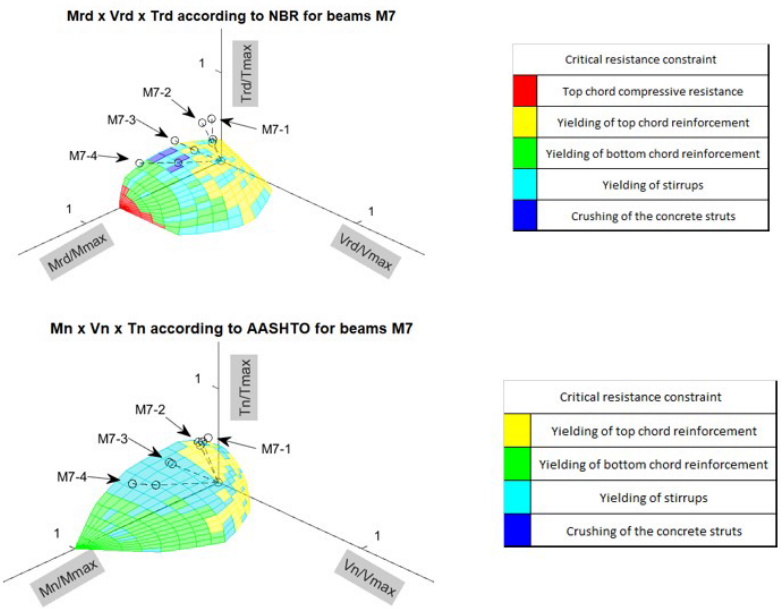

Figure 23: Interaction surface according to NBR and AASHTO for beams M7.

5 CONCLUSIONS

The proposed optimization method development and application for tested beams using prescriptions from NBR 6118/2014 and AASHTO LRFD 2014 allowed to demonstrate its practicality and validity against results from the literature:

- The procedure was efficient and effective in predicting RC beams resistance under combined action for torsion, flexure and shear.
- The program also illustrated the critical resistance mechanism under interaction, aiding the engineer's decision making.
- The performance of both standards on predicting the interaction response of the RC beams was satisfactory when confronted against experimental data.
- NBR 6118/2014 has a much bigger number of equations, which makes its use more complex and may lead to the application of simplified methods.
- AASHTO LRFD 2014, on the other hand, shows a simple and direct general procedure, that analyzes not only failure but the action-strain response.

REFERENCES

[1] E. C. Bentz and M. P. Collins, "Updating the ACI shear design provisions," *Concr. Int.*, vol. 39, no. 9, pp. 33–38, 2017. Accessed: Oct. 4, 2021. [Online]. Available: https://www.concrete.org/publications/internationalconcreteabstractsportal.aspx?m=details&ID=51701012

[2] ACI-ASCE 445 Joint Committee, *Recent Approaches to Shear Design of Structural Concrete*. Farmington Hills, MI, USA: American Concrete Institute, 2000.

[3] ACI-ASCE 445 Joint Committee, *Report on Torsion in Structural Concrete*. Farmington Hills, MI, USA: American Concrete Institute, 2012.

[4] T. T. C. Hsu and Y. L. Mo, *Unified Theory of Concrete Structures.* Hoboken, NJ, USA: Wiley, 2010.

[5] K. N. Rahal, "A unified approach to shear and torsion in reinforced concrete," *Struct. Eng. Mech.*, vol. 77, no. 5, pp. 691–703, 2021, http://dx.doi.org/10.12989/sem.2021.77.5.691.

[6] M. P. Collins, E. C. Bentz, E. G. Sherwood, and L. Xie, "An adequate theory for the shear strength of reinforced concrete structures," *Mag. Concr. Res.*, vol. 60, no. 9, pp. 635–650, 2008, http://dx.doi.org/10.1680/macr.2008.60.9.635.

[7] W. Obel, "Interação torque – cortante: avaliação da NBR-6118," M.S. thesis, Universidade Federal de Pernambuco, Recife, Brasil, 2019.

[8] V. B. Almeida, "Data for: Shear-Torsion-Bending Interaction in RC Beams according to NBR 6118/2014 and AASHTO LRFD 2014." 2022. Accessed: Apr. 15, 2022. [Online]. Available: https://doi.org/10.48331/scielodata.ZGNEIO.

[9] Associação Brasileira de Normas Técnicas, *Projeto de Estruturas de Concreto - Procedimento,* NBR 6118*,* 2014.

[10] J. S. Giongo, *Concreto Armado: Dimensionamento de Elementos Estruturais Fletidos Solicitados por Força Cortante*, 1st ed. São Carlos, Brasil: EESC - Departamento de Engenharia de Estruturas, 2011.

[11] M. S. Ibrahim, E. Gebreyouhannes, A. Muhdin, and A. Gebre, "Effect of concrete cover on the pure torsional behavior of reinforced concrete beams," *Eng. Struct.*, vol. 216, p. 110790, 2020, https://doi.org/10.1016/j.engstruct.2020.110790.

[12] J. K. Wight, *Reinforced Concrete - Mechanics and Design*, 7th ed., Hoboken, NJ, USA: Pearson, 2016.

[13] L. M. Pinheiro, C. D. Muzardo, and S. P. Santos, *Estruturas de Concreto*, 1st ed. São Carlos, Brasil: EESC - Departamento de Engenharia de Estruturas, 2003.

[14] J. S. Giongo, *Dimensionamento Considerando o Estado Limite Último de Elementos Estruturais Lineares Submetidos à Ação de Momento Fletor*, 1st ed. São Carlos, Brasil: EESC - Departamento de Engenharia de Estruturas, 2009.

[15] American Association of State Highway and Transportation Officials, *AASHTO LRFD Bridge Design Specifications,* 7th ed. Washington, DC, USA: AASHTO; 2015.

[16] E. C. Bentz, F. J. Vecchio, and M. P. Collins, "Simplified modified compression field theory for calculating shear strength of reinforced concrete elements," *ACI Struct. J.*, vol. 103, no. 4, pp. 614–624, 2006, http://dx.doi.org/10.14359/16438.

[17] E. C. Bentz and M. P. Collins, "Development of the 2004 Canadian Standards Association (CSA) A23.3 shear provisions for reinforced concrete," *Can. J. Civ. Eng.*, vol. 33, no. 5, pp. 521–534, May 2006, http://dx.doi.org/10.1139/L06-005.

[18] M. P. Collins and D. Mitchell, *Prestressed Concrete Structures.* Englewood Cliffs, NJ, USA: Prentice Hall, 1991.

[19] K. N. Rahal, "Evaluation of AASHTO-LRFD general procedure for torsion and combined loading," *ACI Struct. J.*, vol. 103, no. 5, pp. 683–692, 2006., http://dx.doi.org/10.14359/16920.

[20] H. E. I. Badawy, A. E. McMullen, and I. J. Jordaan, "Experimental investigation of the collapse of reinforced concrete curved beams," *Mag. Concr. Res.*, vol. 29, no. 99, pp. 59–69, 1977, http://dx.doi.org/10.1680/macr.1977.29.99.59.

[21] A. E. McMullen and J. Warwaruk, *The Torsional Strength of Rectangular Reinforced Concrete Beams Subjected to Combined Loading*. Edmonton, Canada: The Univ. Alberta, Dep. Civ. Eng.; 1967. Accessed: Oct. 4, 2021. [Online]. Available: https://era.library.ualberta.ca/items/5086dede-150c-43e1-8a0a-8a0a27d5605f/download/04ed74f7-789e-486d-ba8d-aa3b0ddc554b.

[22] W. M. Onsongo, "Failure interaction curves for combined loading involving torsion, bending, and axial loading," *J. S. Afr. Inst. Civ. Eng.*, vol. 49, no. 1, pp. 17–24, 2007.

Author contributions: V. B. Almeida: Data curation, Formal analysis, Investigation, Methodology, Visualization, Writing-original draft; B. Horowitz: Conceptualization, Project administration, Resources, Supervision, Validation, Writing-review & editing.

Editors: Tulio N. Bittencourt, Guilherme Aris Parsekian